Two Novel Monothiol Glutaredoxins from *Saccharomyces cerevisiae* Provide Further Insight into Iron-Sulfur Cluster Binding, Oligomerization, and Enzymatic Activity of Glutaredoxins†

Nikola Mesecke,‡,§ Sarah Mittler,‡,§ Elisabeth Eckers,‡,§ Johannes M. Herrmann,|| and Marcel Deponte*,‡

Adolf-Butenandt-Institut für Physiologische Chemie, Ludwig-Maximilians Universität D-81377, München, and the Institut für Zellbiologie, Technische Universität Kaiserslautern D-67663, Kaiserslautern, Germany

Received August 31, 2007; Revised Manuscript Received November 9, 2007

ABSTRACT: Two novel monothiol glutaredoxins from yeast (*Sc*Grx6 and *Sc*Grx7) were identified and analyzed in vitro. Both proteins are highly suited to study structure−function relationships of glutaredoxin subclasses because they differ from all monothiol glutaredoxins investigated so far and share features with dithiol glutaredoxins. *Sc*Grx6 and *Sc*Grx7 are, for example, the first monothiol glutaredoxins showing an activity in the standard glutaredoxin transhydrogenase assay with glutathione and bis-(2-hydroxyethyl)-disulfide. Steady-state kinetics of *Sc*Grx7 with glutathione and cysteine-glutathione disulfide are similar to dithiol glutaredoxins and are consistent with a ping-pong mechanism. In contrast to most other glutaredoxins, *Sc*Grx7 and *Sc*Grx6 are able to dimerize noncovalently. Furthermore, *Sc*Grx6 is the first monothiol glutaredoxin shown to directly bind an iron-sulfur cluster. The cluster can be stabilized by reduced glutathione, and its loss results in the conversion of tetramers to dimers. *Sc*Grx7 does not bind metal ions but can be covalently modified in *Escherichia coli* leading to a mass shift of 1090 ± 14 Da. What might be the structural requirements that cause the different properties? We hypothesize that a $G(S/T)X_3$ insertion between a highly conserved lysine residue and the active site cysteine residue could be responsible for the abrogated transhydrogenase activity of many monothiol glutaredoxins. In addition, we suggest an active site motif without proline residues that could lead to the identification of further metal binding glutaredoxins. Such different properties presumably reflect diverse functions in vivo and might therefore explain why there are at least seven glutaredoxins in yeast.

Glutaredoxins (Grxs)[1] are highly conserved throughout evolution and form a group of usually monomeric proteins that structurally belong to the thioredoxin (Trx) superfamily (*1*). Despite their structural similarities, Grxs cover a huge variety of physiological functions, and we are just at the beginning of understanding how these functions are linked to different protein properties: classical Grxs are glutathione: disulfide-oxidoreductases and possess a *C*P(Y/F)*C*-motif at the active site. These enzymes are also called thioltransferases and catalyze the reduction of intra- or intermolecular disulfides at the expense of one or two molecules of reduced glutathione (GSH) (*2*). Recently, two dithiol Grxs—poplar GrxC1 and human Grx2—have been furthermore described to bind iron-sulfur clusters and might function as redox sensors under oxidative stress (*3*−*6*). In both proteins, two Grx subunits are bridged by a [2Fe-2S] cluster that is coordinated by the active site cysteine residues and two molecules of glutathione (*4*−*6*).

Baker's yeast *Saccharomyces cerevisiae* possesses two dithiol Grxs (*Sc*Grx1 and *Sc*Grx2) with a KTY*C*PY*C*-motif at the active site. In vivo studies suggested that both proteins are active in the glutathione:bis-(2-hydroxyethyl)-disulfide transhydrogenase assay (HEDS assay). Yeast strains carrying a double deletion of *SCGRX1* and *SCGRX2* are viable and do not show any reduced growth rate on fermentable/nonfermentable carbon sources or on minimal medium (*7*). Apart from the two classical Grxs, three different monothiol Grxs from yeast have been described so far. *Sc*Grx3, *Sc*Grx4, and *Sc*Grx5 all contain a PK*C*GFSR-motif at the active site (*8*). Mutants lacking *SCGRX3* or *SCGRX4* display no striking growth phenotype in rich or minimal medium, whereas mutants lacking *SCGRX5* grow poorly in minimal medium (*8*). *Sc*Grx5 is a mitochondrial protein with an N-terminal targeting sequence and has been shown to be involved in the synthesis, assembly, or repair of iron-sulfur clusters in vivo (*9*).

Little is known about the enzymatic properties of monothiol Grxs so far. Biochemical analyses revealed that *Sc*Grx5 has a relatively high redox potential (∼175 mV) (*10*) in

† This work was supported by the Deutsche Forschungsgemeinschaft Grant He2803/2-4 and the Stiftung für Innovation Rheinland-Pfalz (J.M.H.).

* To whom correspondence should be addressed. Tel.: 49-89-2180-77122; fax: 49-89-2180-77093; e-mail: marcel.deponte@gmx.de.

‡ Ludwig-Maximilians Universität.

§ These authors contributed equally to this work.

|| Technische Universität Kaiserslautern.

[1] Abbreviations: Grx(s), glutaredoxin(s); *Sc*Grx/*Ec*Grx/*Pf*Grx, glutaredoxin from *Saccharomyces cerevisiae*/*Escherichia coli*/*Plasmodium falciparum*; Trx, thioredoxin; GR, glutathione reductase; HEDS, bis-(2-hydroxyethyl)-disulfide; GSH, reduced glutathione; GSSG, glutathione disulfide; 2-ME, 2-mercaptoethanol; DTT, dithiothreitol; LAA, L-ascorbic acid; GSSEtOH, mixed disulfide between GSH and 2-ME; GSSCys, L-cysteine-glutathione disulfide; Ni-NTA, nickel-nitrilotriacetic acid agarose.

10.1021/bi7017865 CCC: $40.75
Published on Web 01/03/2008

comparison with dithiol Grxs from *Escherichia coli* (−233 and −198 mV for *Ec*Grx1 and *Ec*Grx3^{C65Y}, respectively) (*11*). The thiol group of Cys^{60} at the active site of *Sc*Grx5 has a very low pK_a value of 5.0, and both cysteine residues (Cys^{60} and Cys^{117}) of the protein can be glutathionylated in vitro (*10*); however, Cys^{117} does not seem to be essential for *Sc*Grx5 in vivo (*12*). Although in vivo studies suggested an activity of *Sc*Grx5 in the HEDS assay (*8*), the protein is inactive in vitro (*10*). The situation is similar for the monothiol glutaredoxins 1 and 2 from *Plasmodium falciparum* (*Pf*Glp1 and *Pf*Glp2), having a PL*C*GFS- and PQ*C*KFS-motif, respectively (*13*): Residue Cys^{99} in *Pf*Glp1 and residues Cys^{142} and Cys^{216} in *Pf*Glp2 can be glutathionylated in vitro, and the thiol group of Cys^{99} in *Pf*Glp1 has a pK_a value as low as 5.5. Nevertheless, both *Plasmodium* proteins are inactive in the HEDS assay. In addition, a *Pf*Glp1 mutant with an artificial *C*GF*C*-motif was also found to be inactive, suggesting that additional structural requirements are needed for Grxs to be functional in the HEDS assay (*13*). For further information on monothiol Grxs, see ref *14*.

In the present paper, we describe the first two monothiol Grxs from yeast that are active in the HEDS assay. We named the proteins encoded by the open reading frames YDL010W and YBR014C *Sc*Grx6 and *Sc*Grx7, respectively. *Sc*Grx6 is the first monothiol Grx shown to directly bind an iron-sulfur cluster that is stabilized by reduced glutathione. Furthermore, we show that both proteins are able to form homodimers but have different oligomerization behaviors. The structural requirements for iron-sulfur cluster binding and enzymatic activity are discussed.

MATERIALS AND METHODS

All chemicals used were of the highest purity available. Glutathione reductase (GR) from yeast, GSH, GSSG, dithiothreitol, and NADPH were obtained from Sigma, HEDS was from Alfa Aesar, and L-ascorbic acid was from Merck.

Cloning and Site-Directed Mutagenesis. Using the *Saccharomyces* genome database (http://www.yeastgenome.org/), two open reading frames encoding two uncharacterized nonessential monothiol glutaredoxins on chromosomes II and IV were identified in silico (SGD annotations YBR014C and YDL010W, respectively). Further analyses (http://www.predictprotein.org/) revealed that the N-terminus of both proteins probably contains a transmembrane helix. Therefore, we cloned constructs of *SCGRX*6 and *SCGRX7* encoding N-terminally truncated proteins starting with the residue Val^{34}. The DNA was PCR-amplified and cloned into the *Bam*HI and *Sal*I restriction sites of pQE30 (Qiagen) using the primers 5′GGGGGATCCGTAGAGATAAAAGAGGAAACTTC3′ (ForYDL010w), 5′GGGGTCGACTCAATTATTGGAAGGTTTTTCACG3′ (RevYDL010w), 5′GGGGGATCCGTCAACGAAAGTATTACTACTC3′ (ForYBR014c), and 5′GGGGTCGACCTAGGCACTCTCAGATTGC3′(RevYBR014c). The active site mutant *Sc*Grx6^{C136S} was generated using the QuikChange Site-Directed Mutagenesis Kit (Stratagene) according to the manufacturer's instructions. Mutagenesis primers were 5′GTAAAAGCACGAGCTCATATAGCAAGGGCATGAAGGAACTGCTTG3′ (ForYDL010wMut) and 5′CAAGCAGTTCCTTCATGCCCTTGCTATATGAGCTCGTGCTTTTAC3′ (RevYDL010wMut). Correct insertions and sequences of all constructs were confirmed by sequencing both strands.

Heterologous Expression, Protein Purification, and Detection. N-Terminally MRGS(H)$_6$-tagged constructs were expressed in *E. coli* strain XL1-Blue. Competent cells were transformed prior to each experiment, and suspension cultures were grown at 37 °C to an optical density at 600 nm of 0.5 in Luria−Bertani (LB) medium containing 100 μg/mL ampicillin. Expression was subsequently induced for 4 h with 0.5 mM isopropyl-β-D-1-thiogalactopyranoside (IPTG). Cells from 1 L of culture were harvested by centrifugation at 4 °C (15 min, 4000*g*) and resuspended in 10 mL of buffer containing 50 mM sodium phosphate, 300 mM NaCl, 10 mM imidazole, pH 8.0. Cell walls were digested with lysozyme followed by sonication on ice. The suspension was centrifuged at 4 °C (30 min, 30 500*g*) and loaded on a column containing 1 mL of nickel-nitrilotriacetic acid agarose (Ni-NTA). The recombinant protein was eluted with the same buffer containing 125 mM imidazole. Protein concentrations of the eluates were determined using the Bradford assay with bovine serum albumin as a standard (*15*). Samples were analyzed by gel filtration chromatography and by reducing and nonreducing SDS-PAGE (*16*). Western blots were performed according to the manufacturer's instructions using a mouse penta-His primary antibody (Qiagen) and an anti-mouse IgG secondary antibody conjugated with horseradish peroxidase (Bio-Rad). MALDI-TOF and ESI-TOF mass spectra of intact *Sc*Grx7 were recorded in a central facility of the Ludwig-Maximilians University (http://proteinanalytik.web.med.uni-muenchen.de/).

Gel Filtration Chromatography. Oligomerization of *Sc*Grx6 and *Sc*Grx7 was studied by gel filtration chromatography on a HiLoad 16/60 Superdex 200 prep grade column, which was connected to an ÄKTA-FPLC system (Amersham Pharmacia Biotech). The column was calibrated with a gel filtration standard (Amersham Pharmacia Biotech) and equilibrated with buffer containing 50 mM sodium phosphate or MOPS, 300 mM NaCl, with or without additives (GSH or GSSG), pH 7.4. Protein samples were incubated with the same final concentration of the additives for 4−5 h on ice before application to the column. FPLC fractions were detected photometrically, and peak areas and k_{AV} values were evaluated using the software UNICORN 3.21 (Amersham Pharmacia Biotech). Protein containing FPLC fractions and samples collected prior to the gel filtration were analyzed by reducing and nonreducing SDS-PAGE.

Metal Content Analyses. The metal content of *Sc*Grx6 and *Sc*Grx7 freshly purified from *E. coli* was analyzed in a central facility of the Ludwig-Maximilians University by inductively coupled plasma atomic emission spectroscopy (ICP-AES) using a Varian Vista RL CCD simultaneous ICP-AES spectrometer and the software ICP expert. Eluates from Ni-NTA columns were washed repeatedly with buffer containing 10 mM MOPS, pH 7.4 in a Centriprep YM-10 (Millipore) just before the measurements.

Glutathione:HEDS and Glutathione:GSSCys Transhydrogenase Assays. Steady-state kinetics of *Sc*Grx7 were monitored spectrophotometrically at 25 °C with a thermostated Jasco V-550 UV−vis double beam spectrophotometer. Stock solutions of 4 mM NADPH, 100 mM GSH, 25−125 U/mL GR, and 74 mM HEDS or 10 mM L-cysteine-glutathione disulfide (GSSCys) were freshly prepared in an assay buffer (0.1 M Tris/HCl, 1 mM EDTA, pH 8.0) before each experiment. All assay mixtures contained 0.1 mM NADPH

and 0.25−1.5 U/mL GR To constantly maintain high concentrations of reduced glutathione during the measurements. In separate experiments, we confirmed that GR was not rate-limiting. The final concentration of *Sc*Grx7 was 30−50 nM. For the HEDS assays, either the initial concentration of GSH (between 50 μM and 5 mM) was varied at a fixed initial concentration of HEDS (0.18, 0.37, 0.55, or 0.74 mM) or the initial concentration of HEDS (between 74 μM and 2.2 mM) was varied at a fixed initial concentration of GSH (0.5, 1.0, or 1.5 mM). The consumption of NADPH (ϵ_{340nm} = 6.22 mM^{-1} cm^{-1}) was monitored at 340 nm. A baseline was recorded before the assay was started by the addition of HEDS (see also ref *17*). Alternatively, HEDS, GSH, and NADPH were preincubated for 2 min before GR was added, and the assay was started by the addition of *Sc*Grx7 (see also ref *2*). Assays containing a fixed initial concentration of GSSCys (25, 50, and 100 μM) at variable concentrations of GSH (between 10 and 400 μM) were started by the addition of GSSCys. Measured activities in all assays were corrected (i) by subtracting the absorbance of a reference cuvette containing all components excluding *Sc*Grx7 and (ii) by subtracting the slope (ΔAbs/min) of the baseline. Reaction velocities were plotted according to Michaelis−Menten, Lineweaver−Burk, Eadie−Hofstee, and Hanes theories and were fitted using the program SigmaPlot 10.0 (Systat Software, Inc.). The apparent kinetic parameters K_m^{app} and k_{cat}^{app} were determined by nonlinear regression of Michaelis−Menten plots and by linear regression of the other plots. Values for K_m^{app} and k_{cat}^{app} calculated from the different plots of a single experiment usually varied by less than 10%.

Sequence Alignment and Molecular Modeling. The Protein Data Bank was searched for protein structures containing a thioredoxin fold. Sequences of potential templates were aligned with *Sc*Grx6 and *Sc*Grx7 using the program ClustalW (*18*). Models of monomeric *Sc*Grx6 and *Sc*Grx7 were generated based on the NMR structures of GrxC1 from *Populus tremula* (*4*) (PDB ID 1Z7R). Alignments between template and *Sc*Grx6 or *Sc*Grx7 were optimized manually in the Swiss-PDB Viewer (spdbv). Computations of the models were carried out at the Swiss-Model server using the optimize (project) mode (*19*, *20*). The force field energy of the models was calculated with the GROMOS96 implementation of spdbv.

RESULTS

Sequence Alignments and Molecular Models Suggest Significant Structural Similarities between Dithiol Grxs and ScGrx6 and ScGrx7. What are the structural similarities and differences of *Sc*Grx6, *Sc*Grx7, and monothiol and dithiol Grxs in general? A detailed alignment of monothiol and dithiol Grxs is shown in Supporting Information Figure S1, revealing that monothiol Grxs form a heterogeneous group that can be further subdivided depending on different classification criteria: Several monothiol Grxs possess a (putative) N-terminal mitochondrial targeting sequence (*9*, *21*, *22*), whereas others do not seem to be localized in the mitochondria and might have an N-terminal transmembrane helix (Mesecke, N., et al., unpublished results). Although both proteins possess only one single cysteine residue and are very similar (38% sequence identity), the active site motifs of *Sc*Grx6 and *Sc*Grx7 are different (KSTCSYSK and KTGCPYSK, respectively). Furthermore, *Sc*Grx6 is larger than *Sc*Grx7 because of two insertions between the predicted transmembrane helix and the active site. In contrast to previously studied monothiol Grxs, *Sc*Grx6 and *Sc*Grx7 are more similar to dithiol Grxs since they lack a WP-motif at the glutathione binding site (*13*, *23*) and an insertion before the active site cysteine residue (Figure S1). Many monothiol Grxs contain a conserved arginine residue that could be involved in glutathione binding (*13*, *23*) because the homologous residue Arg^{41} in *Ec*Grx3 was shown to be associated with the carboxylate group of the glycine moiety of glutathione (*24*). However, this arginine residue is replaced with glutamine in *Sc*Grx6 and *Sc*Grx7 (residues Gln^{171} and Gln^{143}, respectively, Figure 1) as well as in many dithiol Grxs (Figure S1). According to molecular models, the glycine carboxylate group of glutathione is presumably associated with the conserved residues Lys^{133} and Lys^{105} of *Sc*Grx6 and *Sc*Grx7 (Figure 1) similar to other Grxs. The carboxylate group of the γ-glutamyl moiety of glutathione could be bound by the less conserved residues Arg^{180} and Arg^{152} of *Sc*Grx6 and *Sc*Grx7 (Figure 1). The side chain of residue Arg^{153} in *Sc*Grx7 might also be involved in glutathione binding swinging between one of the two carboxylate groups. We conclude that *Sc*Grx6 and *Sc*Grx7 form a novel subgroup of monothiol Grxs sharing several structural features with dithiol Grxs.

Cloning, Expression, and Purification. N-Terminally truncated and $MRGS(H)_6$-tagged versions of *Sc*Grx6 and *Sc*Grx7 were successfully expressed and purified from *E. coli* by Ni-NTA affinity chromatography. Since additional bands were detected by reducing SDS-PAGE, eluates of both proteins seemed to contain a few impurities: For *Sc*Grx6, a faint Coomassie-stainable band smaller than 14 kDa was always co-purified (Figure 2A) but could be removed from *Sc*Grx6 by gel filtration. For *Sc*Grx7, a strong double band and a weaker ladder pattern were observed (Figure 2B). Addition of phenylmethylsulfonyl fluoride before cell lysis and sonication did not influence the SDS-PAGE patterns of both proteins. The double band but not the ladder pattern of *Sc*Grx7 could be detected in *E. coli* during IPTG induction by Western blot against the N-terminal His-tag (Figure 2C). Western blots and intact MALDI-TOF mass spectra of *Sc*Grx7 eluates from the Ni-NTA column did also reveal only two proteins with molecular masses of 20 261 ± 48 and 21 351 ± 41 Da resulting in a mass shift of 1090 ± 14 Da (Figure 2D). The calculated molecular mass of 20 241 Da of unmodified *Sc*Grx7 was confirmed by ESI-TOF mass spectrometry, whereas the second protein was not detected (Figure 2E). The additional smaller bands in the *Sc*Grx7 eluate could be partially removed by gel filtration.

ScGrx6 Is an Iron Ion Binding Protein with a Chromophore That Is Stabilized by GSH. During the purification process of *Sc*Grx6 from *E. coli*, we observed that the Ni-NTA resin turned completely brown after protein loading, whereas such changes in color did not occur for $Sc\text{Grx6}^{C136S}$ or *Sc*Grx7. The turquoise color of the resin was only recovered after elution with 125 mM imidazole. Eluates of freshly purified *Sc*Grx6 appeared brownish-orange, and UV−vis spectra revealed a chromophore with an absorbance maximum at 432 nm (Figure 3). No chromophore was observed for $Sc\text{Grx6}^{C136S}$, suggesting that residue Cys^{136} is involved in chromophore binding. The color of *Sc*Grx6 completely faded after a few days. We analyzed the metal

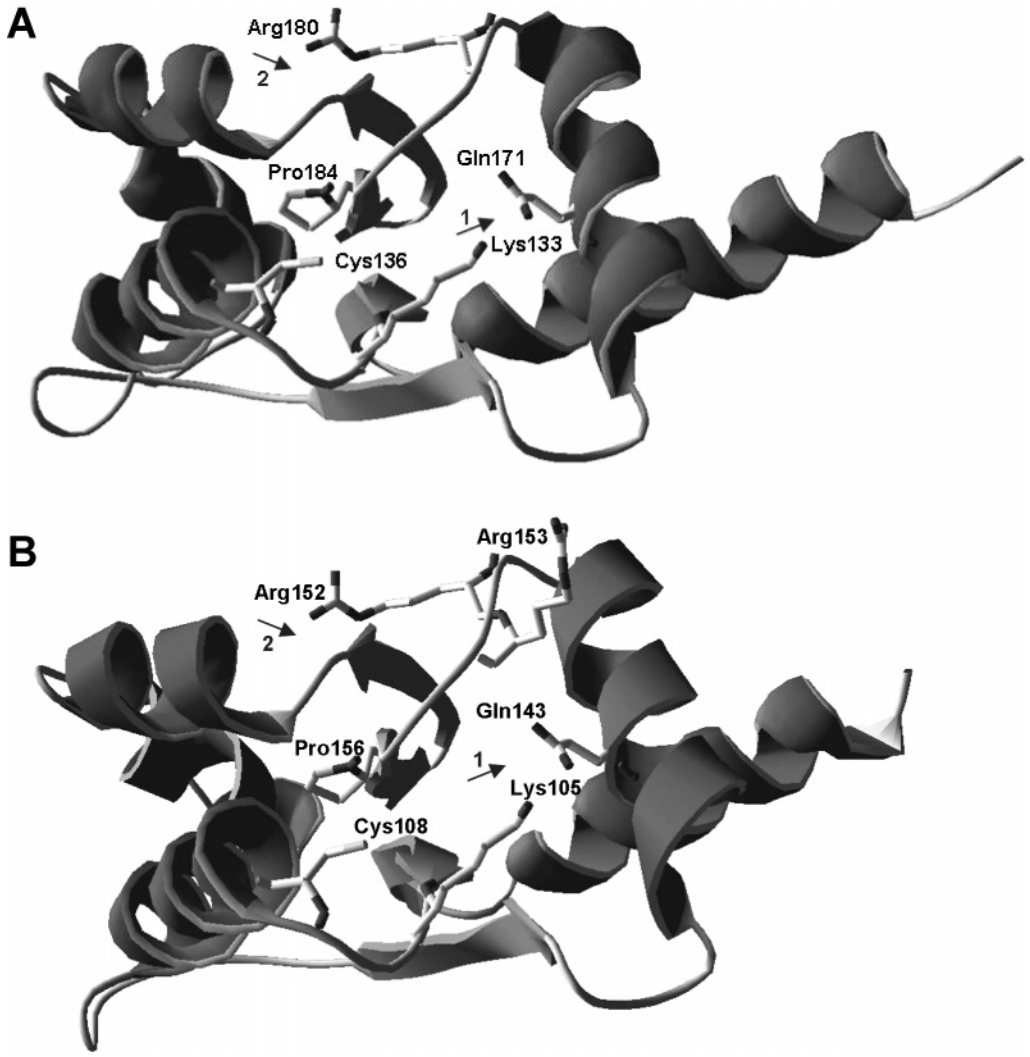

FIGURE 1: Molecular models of *Sc*Grx6 and *Sc*Grx7. Top view of the glutathione binding sites of (A) *Sc*Grx6 and (B) *Sc*Grx7. The force field energies are (A) −3.8 MJ/mol and (B) −3.2 MJ/mol. Residues that are potentially involved in glutathione binding are highlighted. The putative binding site for the carboxylate group of the glycine moiety of glutathione is labeled with arrow 1. The putative binding site for the carboxylate group of the γ-glutamyl moiety of glutathione is labeled with arrow 2.

content of eluates from three independent transformation/expression/purification experiments and detected 0.2−0.3 equiv of iron per protein molecule. No manganese, copper, molybdenum, or cobalt and only very small traces of nickel were detected. In *Sc*Grx7-containing samples, only traces of copper ($\leq$0.02 equiv) were found.

We used the ratio between the absorbances at 278 and 432 nm (Abs_{278nm}/Abs_{432nm}) to compare different expression conditions and potential stabilizing reagents to improve the yield and stability of colored *Sc*Grx6. Values for Abs_{278nm}/Abs_{432nm} of freshly purified protein varied from 15 to 7 depending on the expression. Such a factor of approximately 2 is in accordance with the percentage of the tetramer peak in the gel filtration (20−40%). Best results were obtained expressing *SCGRX6* at 37 °C overnight using LB medium supplemented with 10 μM ferric citrate.

Incubation of freshly purified *Sc*Grx6 at 25 °C in the absence of GSH for 4 h led to an absorbance decrease of 75% (Figure 4A). Addition of reduced glutathione to the incubation mixture led to a stabilization of the chromophore over time, whereas oxidized glutathione (GSSG) did not influence the stability. Addition of L-ascorbic acid and dithiothreitol also slowed down the loss of absorbance, although not as efficiently as GSH (Figure 4A). Monitoring the stability of *Sc*Grx6 for 2 days revealed that the effect of GSH is concentration-dependent (Figure 4B). Furthermore, when freshly purified *Sc*Grx6 was added to buffer containing 10 mM GSH, the absorbance initially seemed to slightly increase.

ScGrx6 and ScGrx7 Are Able To Form Dimers But Have Different Oligomerization Properties. *Sc*Grx6 and *Sc*Grx7 were analyzed by gel filtration chromatography: Freshly purified *Sc*Grx6 eluted at two apparent molecular masses that can be interpreted as dimeric (60−80%) and tetrameric (20−40%) protein subpopulations. Only the tetramer had a strong absorbance at 430 nm (Figure 5A). The presence of 4 mM GSH or 0.5 mM GSSG or the usage of MOPS instead of phosphate buffers did not significantly influence the oligomerization of freshly purified protein, whereas aging caused a loss of the homotetramer (Table 1 and Figure 5B). Both gel filtration peaks contained traces of covalently linked oligomers that were not caused by boiling of the SDS-PAGE samples and that disappeared under reducing conditions (Figure 5C). The tetramer peak contained 0.74 equiv of iron per protein molecule. No iron was detected in the dimer-containing fractions. To test the stability of the oligomers,

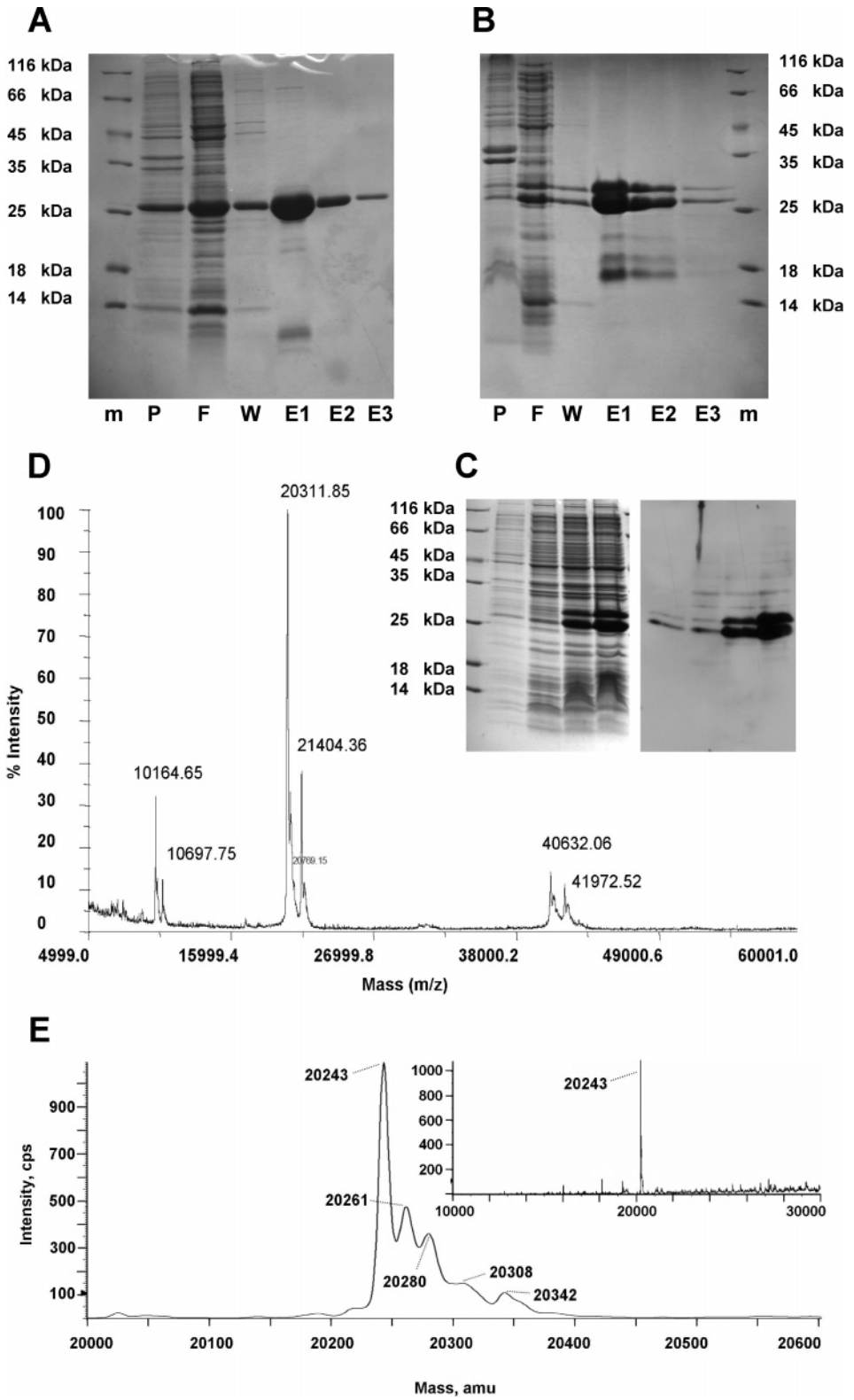

FIGURE 2: Purification of recombinant *Sc*Grx6 and *Sc*Grx7. Both MRGS$(H)_6$-tagged proteins were purified by Ni-NTA affinity chromatography. Eluted fractions were analyzed by reducing SDS-PAGE (15%). Lanes: m, marker; P, pellet; F, flow through; W, 10 mM imidazole wash; and E1−E3, 125 mM imidazole eluates 1−3. (A) Recombinant *Sc*Grx6 (calculated molecular mass of 23.5 kDa) ran at approximately 26 kDa. (B) Recombinant *Sc*Grx7 (calculated molecular mass of 20.2 kDa) ran at approximately 26 and 27 kDa. Three additional bands below 25 kDa were also observed in the eluates. (C) Western blot against the His-tag of *Sc*Grx7. One milliliter of an *E. coli* culture was spun down at four different time points during induction. The cells were directly resuspended in SDS sample buffer, boiled, and subsequently analyzed by SDS-PAGE (left side) and Western blotting (right side). (D) Representative MALDI-TOF mass spectrum of intact *Sc*Grx7 from eluate E1. Two proteins were detected as doubly and singly charged monomers and sometimes also as singly charged dimers. Averaged molecular masses of both proteins were determined to be 20 261 ± 48 and 21 351 ± 41 Da. Small shoulders in the spectrum were due to sinapinic acid and were lost when α-cyano-4-hydroxycinnamic acid was used as a matrix. (E) Representative ESI-TOF mass spectrum of intact *Sc*Grx7 from eluate E1 confirming the calculated molecular mass of unmodified *Sc*Grx7 (20 241 ± 2 Da). Please note that no proteins corresponding to the three additional bands in the SDS gel were observed by mass spectrometry.

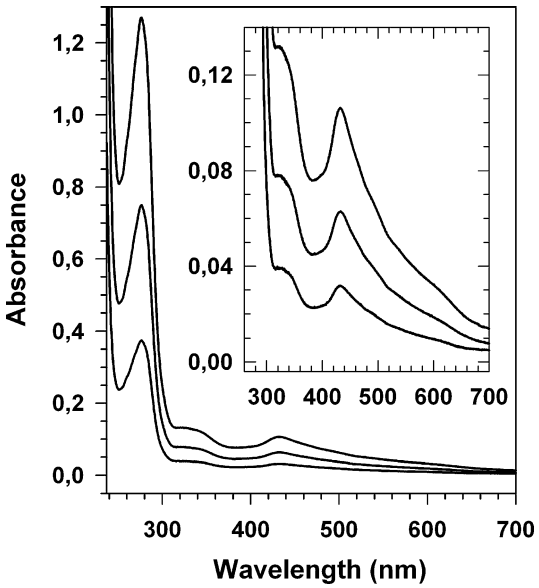

FIGURE 3: UV−vis spectrum of *Sc*Grx6 is very similar to the spectra of the [2Fe-2S] chromophore of dithiol Grxs. Representative spectra of 15, 30, and 55 μM freshly purified *Sc*Grx6. Two local maxima at ~340 and 432 nm were observed. The absorbance of the buffer containing 300 mM sodium chloride, 50 mM sodium phosphate, and 125 mM imidazole, pH 8.0 was subtracted from all spectra.

we separately pooled the tetramer and dimer fractions and reapplied their concentrates to the column. The chromatogram of the reapplied colorless concentrate of the dimer peak showed that the quaternary structure of the protein subpopulation is unchanged. The concentrate of the tetramer fractions was brownish, indicating that the chromophore was tightly bound to *Sc*Grx6 during the gel filtration and concentration procedure. Nevertheless, the tetramer fractions were split up into a tetramer and a dimer peak after reapplication (data not shown).

Freshly purified *Sc*Grx7 eluted with an apparent molecular mass that can be interpreted as a homodimer (Figure 6A). Elution was unchanged in the absence and presence of 2 mM GSH or 0.5 mM GSSG, but aging of *Sc*Grx7 once led to the formation of higher aggregates that can be interpreted as tetramers (Table 2 and Figure 6B). Furthermore, changing the pH from 6 to 8 did not influence oligomerization. At 280 nm, only one peak was detected in the chromatogram of freshly purified protein, whereas at 220 nm, a second, smaller peak with an apparent molecular mass of around 17−19 kDa was observed (Figure 6A). Analyses of the corresponding fractions by SDS-PAGE revealed that the dimer was noncovalently associated since no intermolecular disulfide bonds were detectable when cysteine residues were protected by iodoacetamide before boiling (Figure 6C). The second peak contained the majority of the smaller bands detected by SDS-PAGE (Figures 2B and 6C).

ScGrx6 and ScGrx7 Are the First Monothiol Grxs with Activity in the HEDS Assay. All monothiol Grxs tested so far did not show a significant activity in the HEDS assay, although these proteins could theoretically catalyze the GSH-dependent reduction of bis-(2-hydroxyethyl)-disulfide, for example, through a ping-pong mechanism. We were therefore surprised to find that *Sc*Grx6 and *Sc*Grx7 are both functional in the HEDS assay.

The kinetic data obtained for *Sc*Grx7 could be approximately fitted according to Michaelis−Menten kinetics, with the restriction that enzymatic activity decreased again at high concentrations of HEDS and GSH (Figure 7A). Maximum reaction velocities were proportional to the concentration of *Sc*Grx7 at an enzyme concentration below 50 nM (Figure 7B). A lag phase was observed after the assay was started by adding HEDS (Figure 7C), and we therefore did not evaluate the initial slopes but used ΔAbs/min values obtained 1 min after mixing. In contrast, if the assay was started by the addition of enzyme, no lag phase was observed, and initial reaction velocities were analyzed (Figure 7C).

Activity of *Sc*Grx7 depended (i) on the concentration of HEDS and GSH and (ii) on the assay procedure (Table 3 and Figure 8): Higher activities were obtained when the assay was started by the addition of enzyme (Figure 8A,C) when compared with starting by the addition of HEDS (Figure 8B,D). Varying the concentration of GSH at different initial concentrations of HEDS resulted in rather constant values for K_m^{app} of ~1.3 mM, whereas k_{cat}^{app} increased with increasing concentrations of HEDS (Figure 8A,B). These kinetic patterns did not depend on whether the assay was started with enzyme or HEDS. A constant K_m^{app} and an increasing k_{cat}^{app} value were also observed when the concentration of HEDS was varied at different initial concentrations of GSH and the assay was started by adding enzyme (Figure 8C). However, when assays were started by adding HEDS, varying the concentration of HEDS at different initial concentrations of GSH caused a decrease of K_m^{app} with increasing concentrations of GSH, whereas k_{cat}^{app} was approximately unchanged (Figure 8D and Table 3). None of the Lineweaver−Burk plots is in accordance with a typical ping-pong mechanism (see Discussion).

The kinetic data obtained for *Sc*Grx6 were difficult to fit according to Michaelis−Menten kinetics, presumably due to the inhomogeneous protein population and the instability of the iron-sulfur cluster. Nevertheless, by varying the concentration of GSH at 0.74 mM HEDS, we were able to estimate values for k_{cat}^{app} and K_m^{app} from Lineweaver−Burk plots of 1−2 s^{-1} and 1.5 mM, respectively (data not shown). As a negative control, we used *Sc*Grx6^{C135S}, which was completely inactive. We also analyzed the specific activity of the dimer- and the tetramer-containing fractions from the gel filtration and found that the values for V/[E] of the dimer were about twice as high as for the tetramer. Furthermore, the activity of aged *Sc*Grx6 was higher than for freshly purified protein.

Two-Substrate Kinetics with GSH and GSSCys Suggest a Ping-Pong Mechanism for ScGrx7. Figure 9A shows the parallel line pattern of double reciprocal plots for the variation of GSH concentration at different fixed concentrations of GSSCys. An initial analysis of the apparent kinetic constants using secondary plots revealed a k_{cat} value of 133 s^{-1} and similar K_m values for GSH and GSSCys in the micromolar range (Figure 9B,C). The catalytic efficiency (k_{cat}/K_m) of *Sc*Grx7 was estimated to be approximately 0.5 $\times$ 10^6 M^{-1} s^{-1}. We also analyzed the activity of *Sc*Grx6 and *Sc*Grx7 in the insulin assay (*25*) but detected no significant activity.

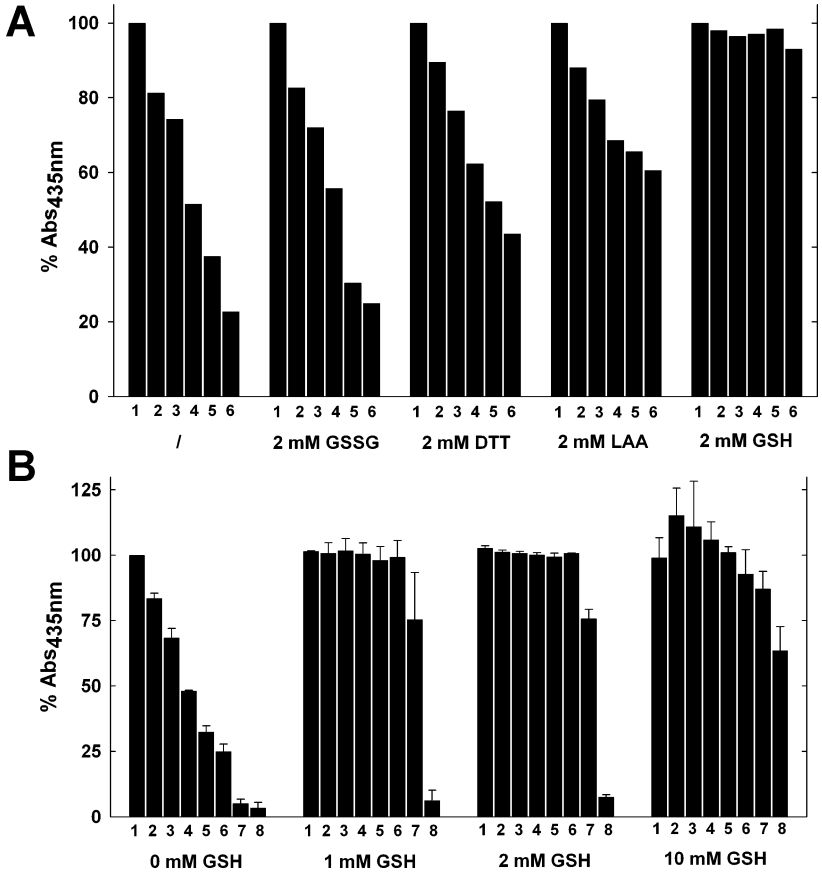

FIGURE 4: *Sc*Grx6 holoprotein is stabilized by the addition of GSH in a concentration-dependent manner. (A) Absorbance of freshly purified *Sc*Grx6 at 435 nm was measured at six different time points in the absence and presence of 2 mM L-ascorbic acid (*LAA*), dithiothreitol (*DTT*), and reduced (*GSH*) and oxidized (*GSSG*) glutathione. The absorbance of the buffer containing 300 mM sodium chloride, 50 sodium phosphate, 125 mM imidazole, 2 mM additive, pH 8.0 was subtracted using a reference cuvette. All assays were performed at 25 °C, and all data points were averaged from two independent transformation/expression/purification experiments. The concentrations of *Sc*Grx6 in the assay were 68 and 72 μM. Time points: 1, 0 h; 2, 0.5 h; 3, 1 h; 4, 2 h; 5, 3 h; and 6, 4 h. The absorbance of the sample without additives at time point 1 was set to 100%. (B) Absorbance of freshly purified *Sc*Grx6 at 435 nm was measured at eight different time points in the absence and presence of three different concentrations of GSH. The absorbance of the buffer containing 300 mM sodium chloride, 50 mM sodium phosphate, 125 mM imidazole, 0−10 mM GSH, pH 8.0 was subtracted using a reference cuvette. All assays were performed at 25 °C, and all data points were averaged from three independent transformation/expression/purification experiments. The concentration of *Sc*Grx6 in the assay was 38−56 μM. Time points: 1, 0 h; 2, 0.5 h; 3, 1 h; 4, 2 h; 5, 3 h; 6, 4 h; 7, 19 h; and 8, 44 h. The absorbance of the sample without GSH at time point 1 was set to 100%.

DISCUSSION

ScGrx7 Is Covalently and Maybe Noncovalently Modified in E. coli. Two major subpopulations of recombinant *Sc*Grx7 were identified by SDS-PAGE, Western blot, and mass spectrometry. The mass shift of 1090 ± 14 Da in the MALDI mass spectrum was probably caused by a covalent secondary modification of the protein in *E. coli*. Modified and unmodified *Sc*Grx7 coeluted from the gel filtration column, suggesting that both proteins were still able to dimerize. A rapid association/dissociation equilibrium between the subunits is one plausible explanation as to why only one peak without additional shoulders (due to the formation of a lighter homodimer of unmodified protein and a heavier homodimer of the modified protein) was observed. We speculate that a large isoprenoid might have been attached to *Sc*Grx7, but so far we were not successful in removing or characterizing the compound despite different approaches (data not shown).

There are two alternative explanations for the weaker, more diffuse bands in the SDS gel below 25 kDa. Since these bands could not be detected by Western blot, we cannot completely rule out an N-terminal processing of *Sc*Grx7 in *E. coli* followed by the co-purification of fragments bound to intact *Sc*Grx7. However, this does not explain (i) the lack of smaller peaks in the mass spectra (Figure 2) and (ii) why the second peak in the gel filtration was only detected at 220 nm (Figure 6A), although aromatic amino acid residues are well-distributed from the N− to the C-terminus of *Sc*Grx7 (Figure S1). Thus, it is likely that noncovalent, Coomassie-stainable, and negatively charged modifications of *Sc*Grx7 caused the pattern of the SDS gel. Whether covalent (and putative noncovalent) modifications point to a physiological role of the protein needs to be studied.

Tetramerization of ScGrx6 Is Coupled to Iron-Sulfur Cluster Binding. UV−vis spectra of the [2Fe-2S]-containing dithiol Grxs from man (*3*) and poplar (*5*) are very similar to the spectra of *Sc*Grx6 (Figure 3). Furthermore, chromophore binding and the presence of iron both depended on the presence of residue Cys^{136} and were restricted to tetrameric *Sc*Grx6. We therefore conclude from our experiments and from the available information on human and poplar Grxs that iron is bound to tetrameric *Sc*Grx6 as an iron-sulfur cluster. Thus, the conversion of labile tetrameric *Sc*Grx6 to a stable dimer was triggered by the loss of the iron-sulfur cluster. The loss was presumably caused by oxidation

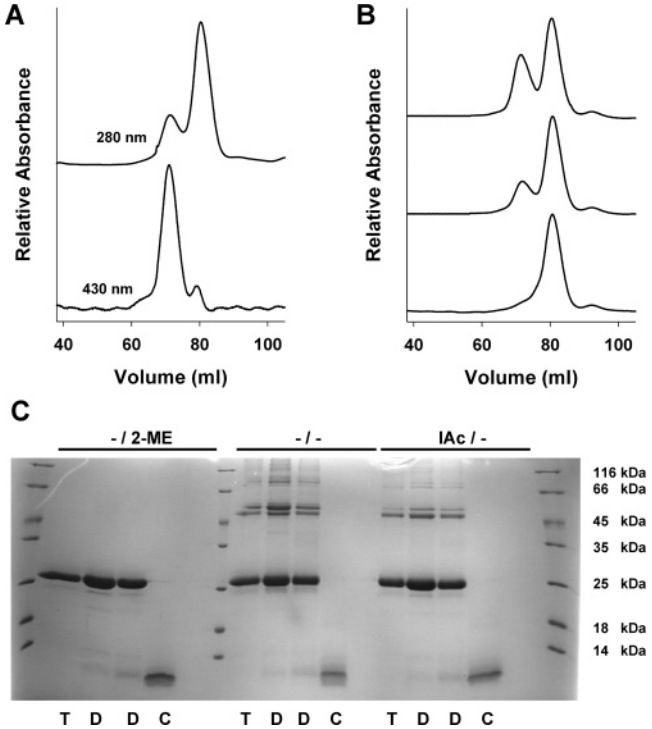

FIGURE 5: *Sc*Grx6 forms labile tetramers and stable dimers. Gel filtration analyses of *Sc*Grx6 purified from *E. coli*. The apparent molecular masses calculated from the chromatograms are listed in Table 1. (A) Freshly purified *Sc*Grx6 formed two at 280 nm detectable subclasses of oligomers (upper chromatogram): a tetramer and a dimer. Using a detection wavelength of 430 nm revealed that the chromophore was mainly bound to the tetramer (lower chromatogram). (B) Aging of *Sc*Grx6 resulted in a loss of the tetramer: chromatograms of samples that were applied to the column 1 h (top), 1 day (middle), or 1 week (bottom) after purification and storage at 4 °C. The detection wavelength was 280 nm. (C) SDS-PAGE analysis of *Sc*Grx6 purified by gel filtration: fractions containing the tetramer *T*, the dimer *D*, and the small Coomassie-stainable band *C* (Figure 2A) were boiled in sample buffer with or without 2-mercaptoethanol (*2-ME*) before SDS-PAGE. To exclude a boiling-induced formation of disulfide bonds, a third sample was pretreated with 2 mM iodoacetamide to block free thiol groups (*IAc*).

Table 1: Data from Representative Gel Filtrations of *Sc*Grx6

buffer composition	No. of peaks at 280 nm	peak area (%)	M_{app} (kDa)	M_{app}/ 23.5 kDa	probable structure
no additives[a]	3	23, 76, 1	119, 54.3, 19.6[b]	5.1, 2.3	$(\alpha_2)_2$, α_2
no additives[c]	3	36, 61, 3	117, 51.4, 18.5[b]	5.0, 2.2	$(\alpha_2)_2$, α_2
no additives[a,d]	2	98, 2	54.8, 20.5[b]	2.3	α_2
no additives[c,d]	2	98, 2	49.6, 18.4[b]	2.1	α_2
4.0 mM GSH[a]	3	20, 78, 2	126, 54.6, 20.4[b]	5.4, 2.3	$(\alpha_2)_2$, α_2
0.5 mM GSSG[a]	3	33, 66, 1	124, 55.7, 20.4[b]	5.3, 2.4	$(\alpha_2)_2$, α_2

[a] 50 mM $Na_xH_yPO_4$, 300 mM NaCl, pH 7.4. [b] Coomassie-stainable band smaller than 14 kDa (as determined by SDS-PAGE). [c] 50 mM MOPS, 300 mM NaCl, pH 7.4. [d] Aged protein sample was applied to the column 1 week after storage at 4 °C without additives.

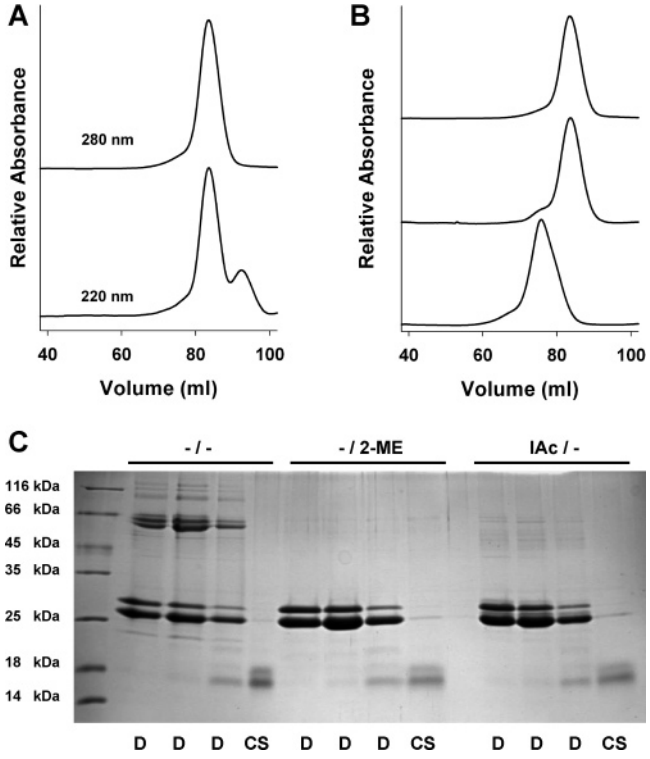

FIGURE 6: *Sc*Grx7 forms stable noncovalently linked dimers. Gel filtration analyses of *Sc*Grx7 purified from *E. coli*. The apparent molecular masses calculated from the chromatograms at 280 nm are listed in Table 2. (A) Freshly purified *Sc*Grx7 eluted in one at 280 nm detectable peak (upper chromatogram), whereas at 220 nm, a second peak was observed (lower chromatogram). (B) Aging of *Sc*Grx7 once resulted in the formation of a putative tetramer: chromatograms of samples that were applied to the column 1 h (top), 1 week (middle), or 1 month (bottom) after purification and storage at 4 °C. (C) SDS-PAGE analysis of *Sc*Grx7 purified by gel filtration: fractions containing the dimer *D* and the smaller Coomassie-stainable bands *CS* (Figure 2B) were boiled in sample buffer with or without 2-mercaptoethanol (*2-ME*) before SDS-PAGE. To exclude a boiling-induced formation of disulfide bonds, a third sample was pretreated with 2 mM iodoacetamide to block free thiol groups (*IAc*).

Table 2: Data from Representative Gel Filtrations of *Sc*Grx7

buffer composition[a]	no. of peaks at 280 nm	peak area (%)	M_{app} (kDa)	M_{app}/ 20.2 kDa	probable structure
no additives	1	~100	42.2	2.1	α_2
no additives[b]	1[c]	<100[c]	43.3	2.1	α_2
no additives[d]	1	~100	88.4	4.4	$(\alpha_2)_2$
0.5 mM GSSG	1	~100	42.0	2.1	α_2
2.0 mM GSH	1	~100	43.0	2.1	α_2

[a] All buffers contained 50 mM $Na_xH_yPO_4$, 300 mM NaCl, pH 7.4. Additives are indicated. [b] Aged protein sample was applied to the column 1 week after storage at 4 °C without additives. [c] Shoulder at a higher molecular mass appeared (Figure 6B). [d] Aged protein sample was applied to the column 1 month after storage at 4 °C without additives.

because GSH but not GSSG stabilized the chromophore. However, the stabilizing effect was not solely restricted to the reducing capacity of GSH since ascorbic acid and dithiothreitol had a much weaker effect (Figure 4A). Our data therefore suggest that GSH could interact with the iron-sulfur cluster as a protective ligand similar to poplar GrxC1 and human Grx2 (*4*−*6*). Further studies are required to confirm iron-sulfur cluster binding to *Sc*Grx6 in vivo.

ScGrx6 and ScGrx7 Are the First Monothiol Grxs Forming Noncovalently Linked Dimers. Grxs lacking an iron-sulfur cluster are usually monomeric. However, using NMR spectroscopy, two monomeric Grxs were also shown to be able to form noncovalently linked dimers (*26*, *27*). Both studied proteins—poplar GrxC4 (*26*) and *Ec*Grx1 (*27*)—are dithiol Grxs. One might argue that gel filtration chromatographical analyses sometimes lead to an incorrect assignment

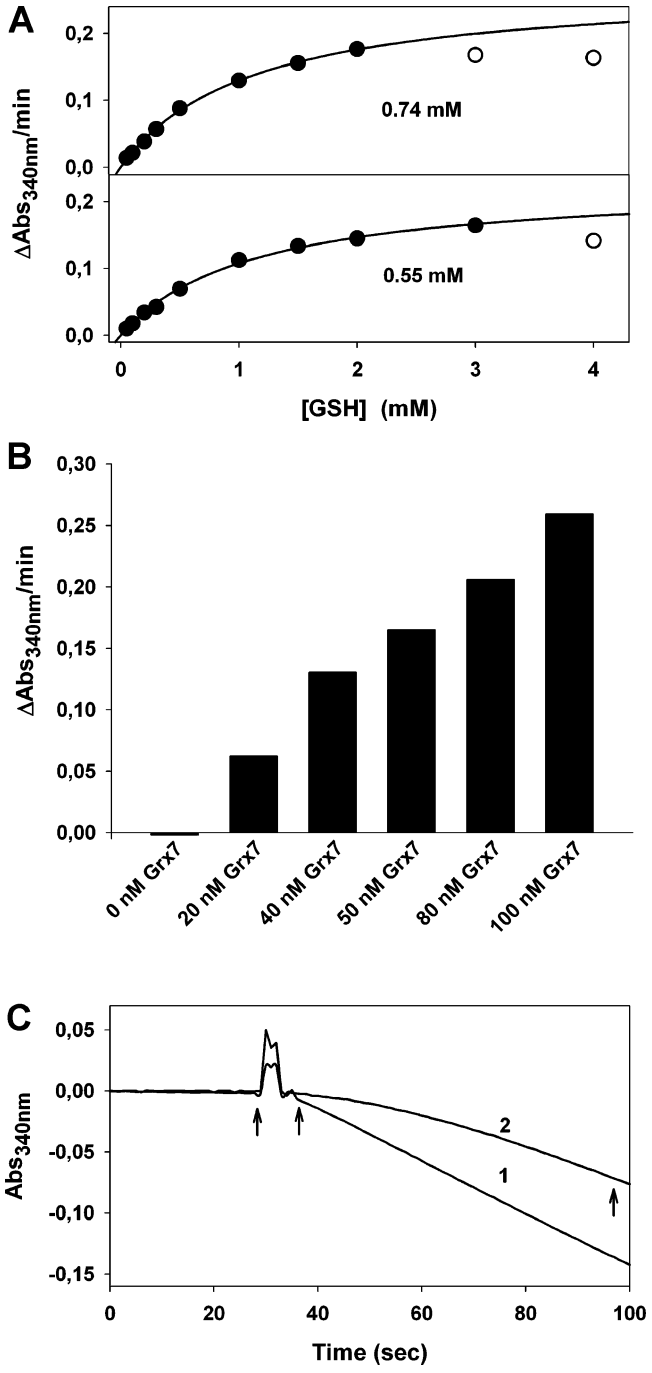

FIGURE 7: *Sc*Grx7 is active in the HEDS assay. The oxidation of NADPH at 25 °C was followed spectrophotometrically at 340 nm (for further details, see Materials and Methods). Assays in panels A and B were started by the addition of HEDS. (A) Michaelis−Menten plots from representative experiments with 0.74 mM (upper panel) and 0.55 mM (lower panel) HEDS. At high concentrations of GSH and HEDS, a decrease of activity is observed. These values (open circles) were excluded from the hyperbolic fit. (B) Measured activity in the HEDS assay depends on the concentration of *Sc*Grx7. (C) Representative time courses of two single measurements: a baseline was recorded for 30 s before the assay was started (first arrow) either by the addition of enzyme (curve 1) or HEDS (curve 2). Reaction velocities were determined either right after mixing (second arrow, curve 1) or 60 s after mixing (third arrow, curve 2) because of an initial lag phase. All reaction velocities were corrected by subtracting the slope of the baseline.

of the quaternary structure of oligomeric proteins and that monomeric *Sc*Grx6 might therefore just have unusual elution properties resulting in apparent dimers. However, the presence of small amounts of covalently linked *Sc*Grx6 dimers in both gel filtration peaks (Figure 5C) excludes this possibility. We therefore conclude from the chromatograms (Figures 5A and 6A) and the SDS gels (Figures 5C and 6C) that *Sc*Grx6 and *Sc*Grx7 are really able to noncovalently dimerize in a GSH- and GSSG-independent manner in vitro. Thus far, it is not known as to which structural differences are responsible for the noncovalent dimerization of *Sc*Grx6 and *Sc*Grx7 in contrast to monomeric Grxs.

Table 3: Apparent Steady-State Kinetic Constants of *Sc*Grx7 Determined from Hanes Plots[a]

variable [GSH]					variable [HEDS]				
[HEDS] (mM)	k_{cat}^{app} (s^{-1})[b]	K_m^{app} (mM)[b]	k_{cat}^{app} (s^{-1})[c]	K_m^{app} (mM)[c]	[GSH] (mM)	k_{cat}^{app} (s^{-1})[b]	K_m^{app} (mM)[b]	k_{cat}^{app} (s^{-1})[c]	K_m^{app} (mM)[c]
0.18	9	1.4	19	1.3	0.5	29	2.2	42	1.4
0.37	14	1.1	35	1.4	1.0	34	1.5	n.d.	n.d.
0.55	19	1.2	n.d.	n.d.	1.5	31	0.8	76	1.4
0.74	23	1.2	44	1.2					

[a] Very similar constants were obtained from Lineweaver−Burk (Figure 8) and Eadie−Hofstee plots. [b] Assays were started at 25 °C by adding *HEDS*. [c] Assays were started at 25 °C by adding *Sc*Grx7.

ScGrx6 But Not ScGrx7 Is Also Able To Dimerize via an Intermolecular Disulfide Bond. In contrast to *Sc*Grx6, dimerization of *Sc*Grx7 was restricted to a noncovalent association because the formation of intermolecular disulfide bonds as detected by nonreducing SDS-PAGE was an artifact due to oxidation of the protein during boiling (Figure 6C). The stable association between different subunits of *Sc*Grx6 (Figure 5C) was not caused by a SDS-resistant iron-sulfur cluster because the same bands of the tetramer fraction were also detectable in the dimer fractions lacking the cluster. Thus, the 2-mercaptoethanol sensitive bands in the SDS gel were due to an intermolecular disulfide bond between two *Sc*Grx6 subunits. It remains unclear as to why more than two bands were detected by nonreducing SDS-PAGE (Figure 5C). *Sc*Grx6 is the second monothiol Grx being able to form covalently linked dimers in vitro and might therefore share mechanistic similarities with *Pf*Glp1 and might be discriminated from other monothiol Grxs (*13*).

Taking into account that a small proportion of *Sc*Grx6 formed covalently linked disulfides (Figure 5C), one can conclude from an iron/protein ratio of 0.74 that one iron ion was bound per cysteine residue in tetrameric *Sc*Grx6. Considering such a stoichiometry, we propose the oligomerization scheme shown in Figure 10: Noncovalently associated dimers are able to oxidize, resulting in an intermolecular disulfide bond, or can bind an iron-sulfur cluster resulting in a bridged dimer of dimers. Since the presence of GSH did stabilize the iron-sulfur cluster but did not shift the ratio between dimeric and tetrameric protein (Table 1), we suggest that one binding site in the putative [2Fe-2S] cluster is not occupied by the protein and can therefore be complexed with GSH.

Steady-State Kinetics Support a Ping-Pong Mechanism for ScGrx7. Gravina and Mieyal performed a detailed analysis of the enzymatic mechanism of dithiol Grxs purified from human red blood cells or rat liver (*17*, *28*): Kinetic data for HEDS and GSH gave sequential patterns (*17*), whereas kinetic data for the reaction between GSSCys and GSH resulted in typical ping-pong patterns (*28*). We obtained very similar results for *Sc*Grx7 (Figures 8 and 9). What caused

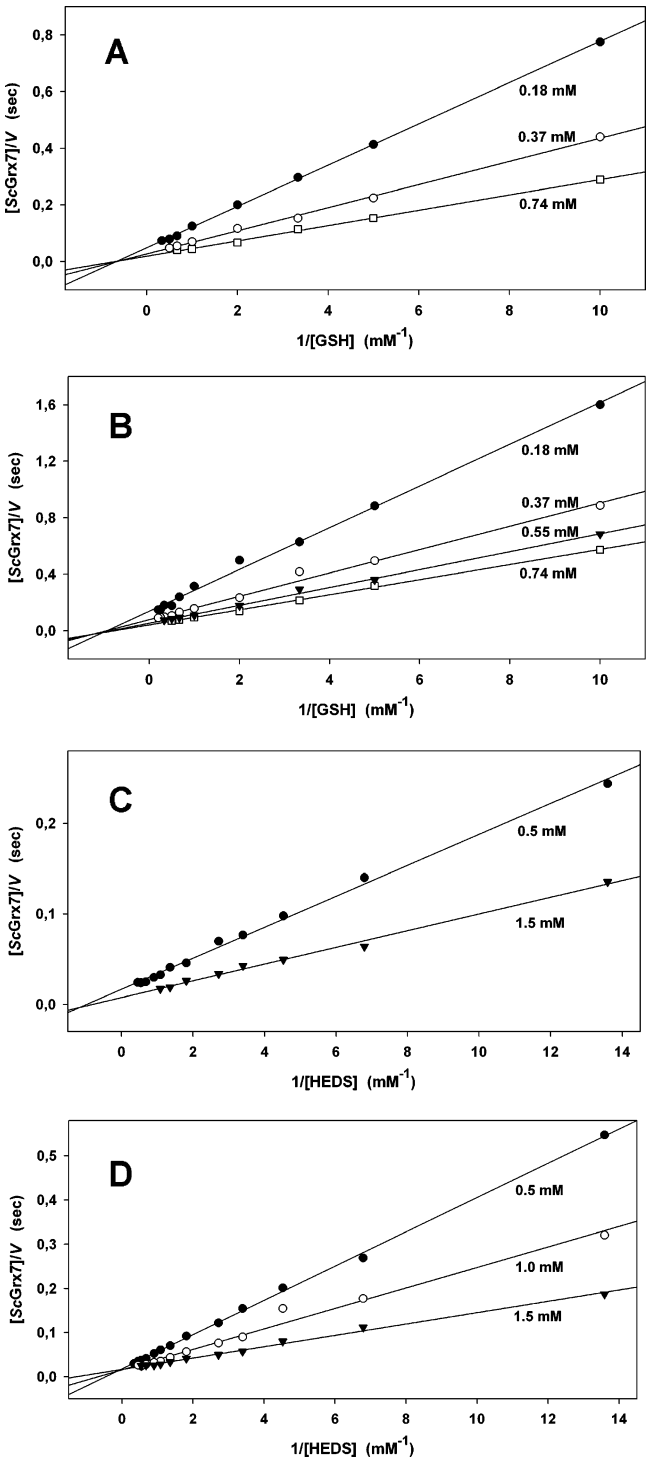

FIGURE 8: Activity of *Sc*Grx7 in the transhydrogenase assay depends on HEDS and GSH. The oxidation of NADPH at 25 °C was followed spectrophotometrically at 340 nm (for further details, see Materials and Methods). Lineweaver−Burk plots from representative experiments are shown. The apparent steady-state kinetic constants are listed in Table 3. (A and B) Concentration of GSH was varied at a fixed concentration of HEDS. The initial millimolar concentration of HEDS is indicated for each series of measurements. (C and D) Concentration of HEDS was varied at a fixed concentration of GSH. The initial millimolar concentration of GSH is indicated for each series of measurements. Assays in panels A and C were started by the addition of *Sc*Grx7, whereas assays in panels B and D were started by adding HEDS.

the different kinetic patterns? It was shown that Grxs catalyze the deglutathionylation of mixed disulfides by transferring the thiol group of GSH to the glutathione sulfur atom of the mixed disulfide substrate (eq 1). A mechanism with a glutathionylated enzyme as an intermediate was proposed (eqs 1a and 1b) (*28*, *29*), thus explaining the observed ping-pong patterns with GSSCys and GSH (*28*) (Figure 9). In contrast, direct reactions between GSH and non-glutathione mixed disulfides were not catalyzed by the enzyme (eq 2) (*28*)

$$\mathrm{RS\mathbf{SG} + GSH \rightarrow RSH + GS\mathbf{SG}} \quad \text{catalyzed by Grx} \quad (1)$$

$$\mathrm{RS\mathbf{SG} + GrxSH \rightarrow RSH + GrxS\mathbf{SG}} \quad \text{ping} \quad (1a)$$

$$\mathrm{GrxS\mathbf{SG} + GSH \rightarrow GrxSH + GS\mathbf{SG}} \quad \text{pong} \quad (1b)$$

$$\mathrm{RSSR + \mathbf{GS}H \rightarrow RSH + RS\mathbf{SG}} \quad \text{nonenzymatic} \quad (2)$$

The observed lag phase and sequential patterns in the HEDS-dependent coupled enzymatic assay (*17*) were therefore suggested to be due to the rate-limiting nonenzymatic formation of the glutathione mixed disulfide (*28*). Indeed, a nonenzymatic formation of the mixed disulfide between GSH and 2-mercaptoethanol (GSSEtOH) is a reasonable explanation for (i) the observed lag phase during our spectrophotometric assays that were started by the addition of HEDS (Figure 7C) and (ii) the increase of k_{cat}^{app} after a preincubation of HEDS and GSH (Table 3). However, starting the assay by the addition of *Sc*Grx7 after preincubation of HEDS and GSH did not result in parallel lines in the Lineweaver−Burk plots (Figure 8A,C) as expected for a ping-pong mechanism with GSSEtOH as the first substrate (eq 1a) and GSH as the second substrate (eq 1b). One might argue that the nonenzymatic reaction between HEDS and GSH was not finished after 2 min preincubation and could therefore be still rate-limiting, although reaction velocities did not further increase after 10 min preincubation in the presence or absence of GR (data not shown). We also confirmed that the back-up system in the coupled assay was not rate-limiting. In summary, we suggest that the sequential kinetic patterns are not necessarily due to the rate-limiting formation of the substrate (eq 2). Further studies are required to check this hypothesis.

Our results are in good agreement with two previous studies on mutated dithiol Grxs from *E. coli* (*29*) and pig liver (*30*) having an artificial CP(Y/F)S-motif. Both proteins were active in the HEDS assay, demonstrating that an intramolecular disulfide bond between the cysteine residues is not required for the catalytic mechanism of dithiol Grxs (*29*, *30*). Nevertheless, we suppose that some details of the mechanisms for dithiol Grxs and *Sc*Grx7 do not have to be identical since dithiol Grxs could form an intramolecular disulfide bond during a side reaction (*28*, *29*). This might explain as to why K_m^{app} and k_{cat}^{app} for HEDS and GSH seem to be variable in the case of the studied dithiol Grxs (*17*), whereas for *Sc*Grx7, one of both values is rather constant (Figure 8 and Table 3).

Lillig and colleagues showed that [2Fe-2S]-containing holo Grx2 is not active in the HEDS assay (*3*) explaining (i) why aged *Sc*Grx6—having lost the iron-sulfur cluster—had a higher activity than freshly purified protein and (ii) why the specific activity of the dimer-containing gel filtration fractions was much higher than in the tetramer-containing fractions (the activity of the tetramer fractions was presumably due to a partial loss of the iron-sulfur cluster during sample preparation). The value for k_{cat}^{app} of *Sc*Grx6 is similar

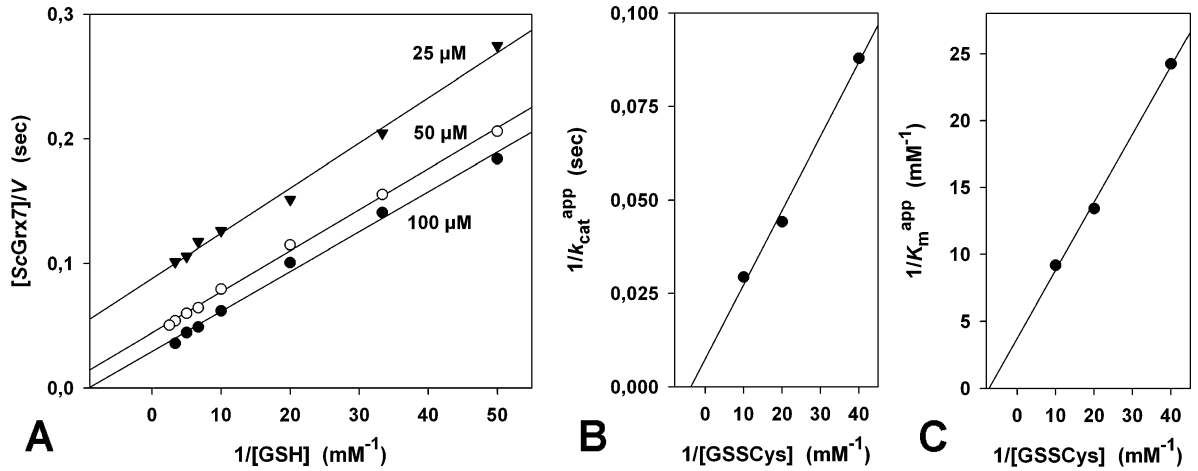

FIGURE 9: Two-substrate kinetics of *Sc*Grx7 with GSSCys and GSH. The oxidation of NADPH at 25 °C was followed spectrophotometrically at 340 nm (for further details, see Materials and Methods). (A) Lineweaver−Burk plot from two initial experiments at three different fixed concentrations of GSSCys is shown. Values for k_{cat} and $K_{m(GSSCys)}$ obtained from panel B are 133 s^{-1} and 265 μM, respectively. Preliminary values for $K_{m(GSH)}$ and $K_{m(GSSCys)}$ obtained from panel C are 266 and 135 μM, respectively.

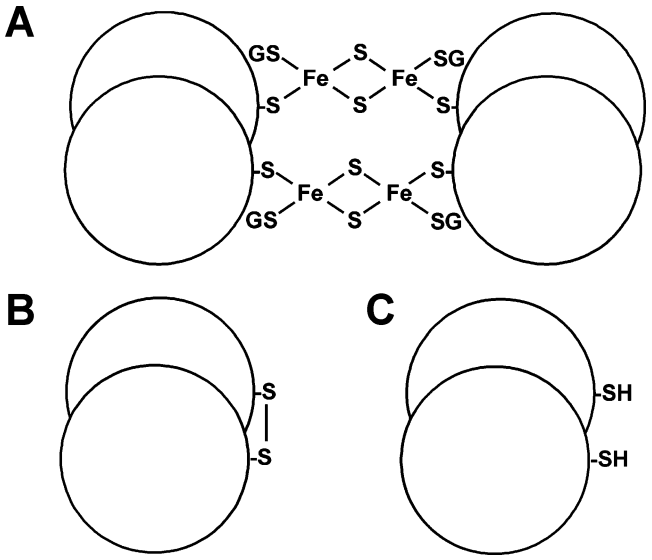

FIGURE 10: Model of the alternative *Sc*Grx6 quaternary structures. Two subunits in tetrameric (A), oxidized dimeric (B), and reduced dimeric (C) *Sc*Grx6 are noncovalently associated via the same dimerization interface. In addition, two subunits can be bridged by a putative [2Fe-2S] cluster (A) or by an intermolecular disulfide bond (B). A loss of the iron-sulfur cluster leads to the dissociation of the tetramer into dimers. The iron-sulfur cluster is presumably liganded by glutathione (*GS*).

to human apo Grx2 (*3*), whereas *Sc*Grx7 is about 40−80 times more active at identical assay conditions.

Structural Features That Are Required for Enzymatic Activity and Iron-Sulfur Cluster Binding. What might be the structural difference between monothiol Grxs with or without activity in the HEDS assay? All inactive monothiol Grxs, such as Grx4 from *E. coli* (*31*), Glps from *P. falciparum* (*13*, *21*), and Grx3−5 from yeast (*10*, *14*), possess (i) a WP-motif and (ii) an insertion between a highly conserved lysine residue and the active site cysteine residue (Figure S1). Molecular models and glutathionylation studies on *P. falciparum* monothiol Grxs (*13*) and *Sc*Grx5 (*10*) as well as the solution structure of *Ec*Grx4 (*23*) support the assumption that the WP-motif does not inhibit glutathione binding. We therefore suggest that the insertion could be responsible for the abrogated activity of this large subgroup of inactive monothiol Grxs. Further studies are underway to test the hypothesis.

Why do some Grxs bind iron-sulfur clusters, whereas others do not? What are the common structural elements of the iron-sulfur cluster binding mono- and dithiol Grxs *Sc*Grx6, poplar GrxC1 (*4*, *5*), and Grx2 from man (*3*, *6*)? All of these proteins have two features in common: (i) no G(S/T)x_3 insertion after the highly conserved lysine residue and (ii) no proline residues around the (N-terminal) cysteine residue (Figure S1). The G(S/T)x_3 insertion cannot be the cause for an inhibited iron-sulfur cluster binding because many dithiol Grxs do not bind iron-sulfur clusters, although they lack the insertion. In contrast, proline residues in a PxC- or CP-motif at the active site are present in all mono- and dithiol Grxs that do not seem to bind iron-sulfur clusters. We therefore hypothesize that further Grxs sharing a SK-(S/T)(S/T)***C***(S/G)(Y/F)(C/S)-motif are probably also iron-sulfur cluster binding proteins and might be identified in silico. Recently, Su and colleagues suggested that a highly conserved *cis*-proline residue in members of the thioredoxin family can also preclude metal binding (*32*). It might therefore be interesting to analyze as to why *Sc*Grx6, GrxC1, and human Grx2—having the conserved proline residue (Figure S1)—are nevertheless binding an iron-sulfur cluster.

CONCLUSION

The two novel monothiol Grxs from yeast *Sc*Grx6 and *Sc*Grx7 are very different from other monothiol Grxs studied so far. Both proteins rather share several features with dithiol Grxs such as an glutathione:disulfide-oxidoreductase activity in the HEDS assay and a lacking G(S/T)x_3 insertion between a conserved lysine residue and the active site cysteine residue. In addition, *Sc*Grx6 binds an iron-sulfur cluster that is stabilized by GSH in similarity to poplar GrxC1 and human Grx2. So far, the quaternary structures of *Sc*Grx6 and *Sc*Grx7 are unique among Grxs. Furthermore, the predicted transmembrane helices, the putative non-mitochondrial localization, and secondary modifications together are exemplary for the high diversity of Grxs and point to novel physiological functions partially explaining as to why yeast has seven Grxs.

ACKNOWLEDGMENT

The authors thank Sandra Esser for her excellent technical assistance, Axel Imhof and Lars Israel for mass spectrometry results, Helmut Hartl for atomic emission spectroscopy results, and Prof. Walter Neupert for his support. We are very grateful to Prof. John Mieyal for providing us with L-cysteine-glutathione disulfide.

SUPPORTING INFORMATION AVAILABLE

Detailed alignment of monothiol and dithiol Grxs for comparison. This material is available free of charge via the Internet at http://pubs.acs.org.

REFERENCES

1. Martin, J. L. (1995) Thioredoxin: A fold for all reasons, *Structure 15*, 245−250.
2. Holmgren, A., and Aslund, F. (1995) Glutaredoxin, *Methods Enzymol. 252*, 283−292.
3. Lillig, C. H., Berndt, C., Vergnolle, O., Lonn, M. E., Hudemann, C., Bill, E., and Holmgren, A. (2005) Characterization of human glutaredoxin 2 as iron-sulfur protein: A possible role as redox sensor, *Proc. Natl. Acad. Sci. U.S.A. 102*, 8168−8173.
4. Feng, Y., Zhong, N., Rouhier, N., Hase, T., Kusunoki, M., Jacquot, J. P., Jin, C., and Xia, B. (2006) Structural insight into poplar glutaredoxin C1 with a bridging iron-sulfur cluster at the active site, *Biochemistry 45*, 7998−8008.
5. Rouhier, N., Unno, H., Bandyopadhyay, S., Masip, L., Kim, S. K., Hirasawa, M., Gualberto, J. M., Lattard, V., Kusunoki, M., Knaff, D. B., Georgiou, G., Hase, T., Johnson, M. K., and Jacquot, J. P. (2007) Functional, structural, and spectroscopic characterization of a glutathione-ligated [2Fe-2S] cluster in poplar glutaredoxin C1, *Proc. Natl. Acad. Sci. U.S.A. 104*, 7379−7384.
6. Johansson, C., Kavanagh, K. L., Gileadi, O., and Oppermann, U. (2007) Reversible sequestration of active site cysteines in a 2Fe-2S-bridged dimer provides a mechanism for glutaredoxin 2 regulation in human mitochondria, *J. Biol. Chem. 282*, 3077−3082.
7. Luikenhuis, S., Perrone, G., Dawes, I. W., and Grant, C. M. (1998) The yeast *Saccharomyces cerevisiae* contains two glutaredoxin genes that are required for protection against reactive oxygen species, *Mol. Biol. Cell 9*, 1081−1091.
8. Rodriguez-Manzaneque, M. T., Ros, J., Cabiscol, E., Sorribas, A., and Herrero, E. (1999) Grx5 glutaredoxin plays a central role in protection against protein oxidative damage in *Saccharomyces cerevisiae*, *Mol. Cell Biol. 19*, 8180−8190.
9. Rodriguez-Manzaneque, M. T., Tamarit, J., Belli, G., Ros, J., and Herrero, E. (2002) Grx5 is a mitochondrial glutaredoxin required for the activity of iron/sulfur enzymes, *Mol. Biol. Cell 13*, 1109−1121.
10. Tamarit, J., Belli, G., Cabiscol, E., Herrero, E., and Ros, J. (2003) Biochemical characterization of yeast mitochondrial Grx5 monothiol glutaredoxin, *J. Biol. Chem. 278*, 25745−25751.
11. Aslund, F., Berndt, K. D., and Holmgren, A. (1997) Redox potentials of glutaredoxins and other thiol-disulfide oxidoreductases of the thioredoxin superfamily determined by direct protein−protein redox equilibria, *J. Biol. Chem. 272*, 30780−30786.
12. Belli, G., Polaina, J., Tamarit, J., De La Torre, M. A., Rodriguez-Manzaneque, M. T., Ros, J., and Herrero, E. (2002) Structure−function analysis of yeast Grx5 monothiol glutaredoxin defines essential amino acids for the function of the protein, *J. Biol. Chem. 277*, 37590−37596.
13. Deponte, M., Becker, K., and Rahlfs, S. (2005) *Plasmodium falciparum* glutaredoxin-like proteins, *Biol. Chem. 386*, 33−40.
14. Herrero, E., and de la Torre-Ruiz, M. A. (2007) Monothiol glutaredoxins: A common domain for multiple functions, *Cell. Mol. Life Sci. 64*, 1518−1530.
15. Bradford, M. M. (1976) A rapid and sensitive method for the quantitation of microgram quantities of protein utilizing the principle of protein−dye binding, *Anal. Biochem. 72*, 248−254.
16. Laemmli, U. K. (1970) Cleavage of structural proteins during the assembly of the head of bacteriophage T4, *Nature (London, U.K.) 227*, 680−685.
17. Mieyal, J. J., Starke, D. W., Gravina, S. A., and Hocevar, B. A. (1991) Thioltransferase in human red blood cells: Kinetics and equilibrium, *Biochemistry 30*, 8883−8891.
18. Thompson, J. D., Higgins, D. G., and Gibson, T. J. (1994) CLUSTAL W: Improving the sensitivity of progressive multiple sequence alignment through sequence weighting, position-specific gap penalties, and weight matrix choice, *Nucleic Acids Res. 22*, 4673−4680.
19. Guex, N., and Peitsch, M. C. (1997) SWISS-MODEL and the Swiss-PdbViewer: An environment for comparative protein modeling, *Electrophoresis 18*, 2714−2723.
20. Schwede, T., Kopp, J., Guex, N., and Peitsch, M. C. (2003) SWISS-MODEL: An automated protein homology-modeling server, *Nucleic Acids Res. 31*, 3381−3385.
21. Rahlfs, S., Fischer, M., and Becker, K. (2001) *Plasmodium falciparum* possesses a classical glutaredoxin and a second, glutaredoxin-like protein with a PICOT homology domain, *J. Biol. Chem. 276*, 37133−37140.
22. Wingert, R. A., Galloway, J. L., Barut, B., Foott, H., Fraenkel, P., Axe, J. L., Weber, G. J., Dooley, K., Davidson, A. J., Schmid, B., Paw, B. H., Shaw, G. C., Kingsley, P., Palis, J., Schubert, H., Chen, O., Kaplan, J., and Zon, L. I. (2005) Deficiency of glutaredoxin 5 reveals that Fe-S clusters are required for vertebrate haem synthesis, *Nature (London, U.K.) 436*, 1035−1039.
23. Fladvad, M., Bellanda, M., Fernandes, A. P., Mammi, S., Vlamis-Gardikas, A., Holmgren, A., and Sunnerhagen, M. (2005) Molecular mapping of functionalities in the solution structure of reduced Grx4, a monothiol glutaredoxin from *Escherichia coli*, *J. Biol. Chem. 280*, 24553−24561.
24. Aslund, F., Nordstrand, K., Berndt, K. D., Nikkola, M., Bergman, T., Ponstingl, H., Jornvall, H., Otting, G., and Holmgren, A. (1996) Glutaredoxin-3 from *Escherichia coli*. Amino acid sequence, ^{1}H and ^{15}N NMR assignments, and structural analysis, *J. Biol. Chem. 271*, 6736−6745.
25. Holmgren, A. (1979) Thioredoxin catalyzes the reduction of insulin disulfides by dithiothreitol and dihydrolipoamide, *J. Biol. Chem. 254*, 9627−9632.
26. Noguera, V., Walker, O., Rouhier, N., Jacquot, J. P., Krimm, I., and Lancelin, J. M. (2005) NMR reveals a novel glutaredoxin−glutaredoxin interaction interface, *J. Mol. Biol. 353*, 629−641.
27. Kelley, J. J., Caputo, T. M., Eaton, S. F., Laue, T. M., and Bushweller, J. H. (1997) Comparison of backbone dynamics of reduced and oxidized *Escherichia coli* glutaredoxin-1 using ^{15}N NMR relaxation measurements, *Biochemistry 36*, 5029−5044.
28. Gravina, S. A., and Mieyal, J. J. (1993) Thioltransferase is a specific glutathionyl mixed disulfide oxidoreductase, *Biochemistry 32*, 3368−3376.
29. Bushweller, J. H., Aslund, F., Wuthrich, K., and Holmgren, A. (1992) Structural and functional characterization of the mutant *Escherichia coli* glutaredoxin (C14 → S) and its mixed disulfide with glutathione, *Biochemistry 31*, 9288−9293.
30. Yang, Y. F., and Wells, W. W. (1991) Identification and characterization of the functional amino acids at the active center of pig liver thioltransferase by site-directed mutagenesis, *J. Biol. Chem. 266*, 12759−12765.
31. Fernandes, A. P., Fladvad, M., Berndt, C., Andresen, C., Lillig, C. H., Neubauer, P., Sunnerhagen, M., Holmgren, A., and Vlamis-Gardikas, A. (2005) A novel monothiol glutaredoxin (Grx4) from *Escherichia coli* can serve as a substrate for thioredoxin reductase, *J. Biol. Chem. 280*, 24544−24552.
32. Su, D., Berndt, C., Fomenko, D. E., Holmgren, A., and Gladyshev, V. N. (2007) A conserved *cis*-proline precludes metal binding by the active site thiolates in members of the thioredoxin family of proteins, *Biochemistry 46*, 6903−6910.

BI7017865